Nonlinear Dynamics **22:** 29–38, 2000.

Elliptic Curves and Three-Dimensional Flow Patterns

BRIAN J. CANTWELL
Department of Aeronautics and Astronautics, Stanford University, Stanford, CA 94305, U.S.A.

(Received: 15 March 1999; accepted: 16 April 1999)

Abstract. This paper is concerned with the geometry of flow patterns in the classical problem of an impulsely-started, incompressible, axisymmetric, laminar jet generated by a point force. The second and third invariants of the velocity gradient tensor, evaluated at critical points in the jet, describe the fundamental dependence of the flow on the jet Reynolds number. As the Reynolds number is increased from zero to infinity, the critical points follow elliptic curves in the space of invariants and rational roots occur at bifurcation points in this space. The corresponding invariants of the acceleration gradient tensor trace out a trajectory with infinitely many, densely spaced rational roots. The results provide new insight into the viscous and pressure forces which act in the jet and the balance between strain and rotation which leads to the onset of a starting vortex.

Keywords: Fluid mechanics, turbulence, transition, elliptic curves, critical points, flow patterns, velocity gradient, round jet, bifurcation.

1. Introduction

Direct numerical simulations of turbulent flow provide an opportunity to study the physics of fluid flow at unprecedented levels of detail. Instantaneous vector fields of velocity, pressure gradient, temperature gradient and concentration gradient can be readily accessed. However the complexity of these fields is such that efficient, reference frame independent, means are required in order to identify significant features without having to visualize the entire data set. This has led to the development of a hybrid physical-statistical method [1–4] based on an approach where the flow is studied in the space of invariants of the gradient tensor of the flow variable in question (velocity gradient, pressure gradient-gradient, temperature gradient-gradient and concentration gradient-gradient). In a three-dimensional flow the eigenvalues of the gradient tensor satisfy a cubic equation

$$\lambda^3 + P\lambda^2 + Q\lambda + R = 0, \tag{1}$$

where P, Q and R are the invariants. The eigenvalues change from real to complex across the surface where the cubic discriminant,

$$D = \frac{27}{4}R^2 + \left(P^3 - \frac{9}{2}PQ\right)R + Q^2\left(Q - \frac{1}{4}P^2\right) \tag{2}$$

changes sign. The invariants determine the local structure of the flow in the neighborhood of the point where the gradient tensor is evaluated. When the invariants are determined over the whole flow, as in a typical computational field, the entire topological structure of the vector field is defined.

The prototypical example of this method is the unsteady laminar round jet discussed in [5]. The round jet is self-similar in time allowing the global flow structure to be determined just from a consideration of isolated critical points in the vector field of particle paths in similarity coordinates [6–10]. The present paper expands on the discussion of the algebraic characteristics of the velocity gradient tensor evaluated at the critical points of the jet and depicted in figures 1–3 of [5]. In particular, I would like to describe the relationship between the invariants of the velocity gradient tensor and elliptic curves.

2. Flow Patterns in the Round Jet Depicted in Reference [5]

Figures 1–3 in [5] (see also [7–9] and figures 4–6 in [7]) depict a computation of the flow produced by an impulsively started laminar round jet at three Reynolds numbers. Each figure shows contours of the stream function and the vorticity. Figures 1c–3c show particle paths in similarity coordinates. Figure 3c shows fluid being stretched at an on-axis saddle and then entrained into a stable focus of particle paths. Intuition would suggest that such a roll-up of fluid should occur together with a concentration of the vorticity. In fact, the stable focus occurs in a region where the vorticity decays smoothly and monotonically as can be seen in figure 3b. There is no local concentration of vorticity anywhere in the flow but at the source of the jet. So how does the roll-up depicted in figures 2 and 3 of [5] occur?

3. The Space of Invariants

The answer has to do with the balance between rotation and strain implicit in the invariants Q and R. In Figures 1a and 1b of the present paper the Reynolds number dependence of the flow is shown in the space of invariants of the velocity gradient tensor evaluated at the critical points of the jet. The correspondence between local patterns in the vector field and the invariants is discussed at length in [2] and especially [11]. Actually two vector fields need to be considered; the velocity field and the vector field of particle paths. The problem of the unsteady round jet is invariant under the one-parameter dilation group,

$$\left.\begin{aligned} \overline{x}^i &= e^a x^i; \qquad \overline{t} = e^{2a} t \\ \overline{u}^i &= e^{-a} u^i; \qquad \frac{\overline{p}}{\rho} = e^{-2a} \frac{p}{\rho} \end{aligned}\right\}. \tag{3}$$

Invariants of this group form the similarity variables of the solution,

$$\left.\begin{aligned} u^i &= \nu^{1/2} t^{-1/2} U^i(\xi) \\ \frac{p}{\rho} &= \nu t^{-1} P(\xi) \\ \xi^j &= x^j / (\nu t)^{1/2} \end{aligned}\right\}. \tag{4}$$

The Reynolds number is

$$R_e = \frac{\sqrt{J/\rho}}{\nu}, \tag{5}$$

where J is the force which creates the jet. The U^i and P are self-similar velocities and kinematic pressure. The similarity form of the velocity gradient tensor is

$$a^i_j = \frac{\partial u^i}{\partial x^j} = \frac{1}{t}\frac{\partial U^i}{\partial \xi^j} = \frac{1}{t}A^i_j(\xi). \tag{6}$$

Note that the value of the dimensioned velocity gradient tensor does not depend on J/ρ or ν. Therefore an observer moving at a fixed ξ can use the current value of the velocity gradient as a clock to determine the age of the flow regardless of the flow Reynolds number. The particle path equations,

$$\frac{\mathrm{d}x^i}{\mathrm{d}t} = u^i(x,t), \tag{7}$$

when transformed to similarity variables become

$$\frac{\mathrm{d}\xi^i}{\mathrm{d}\tau} = U^i(\xi;\mathrm{Re}) - \frac{1}{2}\xi^i, \tag{8}$$

where $\tau = \ln t$. The vector field depicted in figures 1c–3c of [5] is the right-hand side of (8). Note that these patterns, like the gradient tensor itself, do not depend on the observer as discussed in [5].

Critical points occur where the right-hand side of (8) is equal to zero,

$$U^i(\xi_c;\mathrm{Re}) - \frac{1}{2}\xi^i_c = 0. \tag{9}$$

The solution for the jet is expanded in a Taylor series near the critical points and the gradient tensor of particle paths is determined. When the invariants of

$$M^i_j = A^i_j - \frac{1}{2}\delta^i_j, \tag{10}$$

are evaluated at various Reynolds numbers the result is the trajectories of the critical points shown in Figures 1a and 1b. The arrows in these figures indicate the direction of increasing Reynolds number. The first invariants of A and M are

$$P_M = \frac{3}{2}; \quad P_A = 0. \tag{11}$$

The second and third invariants (Q, R) are expressed in terms of matrix elements,

$$\left.\begin{aligned} Q_A &= -\frac{1}{2}A^i_k A^k_i \\ Q_M &= \frac{9}{8} - \frac{1}{2}M^i_k M^k_i \end{aligned}\right\} \tag{12}$$

and

$$\left.\begin{aligned} R_A &= -\frac{1}{3}A^i_k A^k_j A^j_i \\ R_M &= -\frac{1}{3}M^i_k M^k_j M^j_i + \frac{3}{2}Q_M - \frac{9}{8} \end{aligned}\right\}. \tag{13}$$

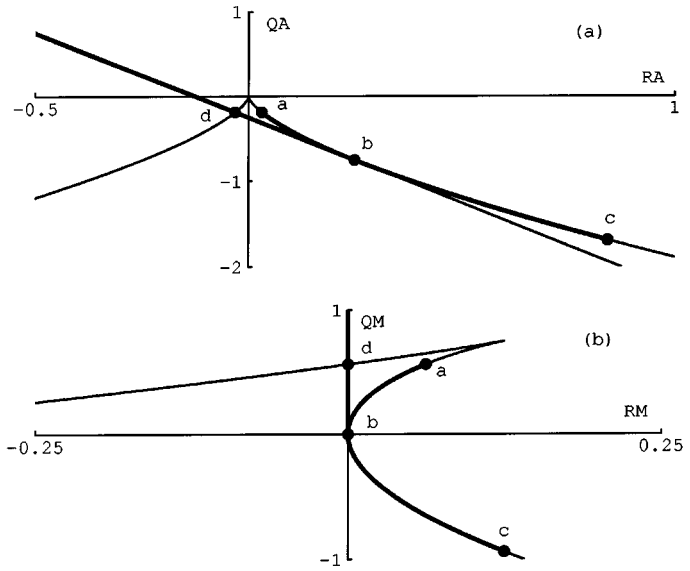

Figure 1. Critical point trajectories in the round jet. (a) The trajectory in $Q_A R_A$ at various R_e. (b) The same trajectory in $Q_M R_M$.

It is worth noting that quite often the values of the invariants can be determined without a complete knowledge of the solution [9]. The invariants of M and A are related to one another as follows

$$\left.\begin{aligned} Q_M &= Q_A + \frac{3}{4} \\ R_M &= R_A + \frac{1}{2}Q_A + \frac{1}{8} \end{aligned}\right\}. \tag{14}$$

The discriminant of A is

$$D_A = Q_A^3 + \frac{27}{4}R_A^2 \tag{15}$$

and the discriminant of M is

$$D_M = Q_M^3 + \frac{27}{4}R_M^2 + \frac{27}{4}R_M\left(\frac{1}{2} - Q_M\right) - \frac{9}{16}Q_M^2. \tag{16}$$

The latter relationship is Equation (2) with $P = 3/2$. If $D > 0$ the eigenvalues are complex and vorticity dominates strain. If $D < 0$ the eigenvalues are real and strain dominates vorticity. A complete road map to (P, Q, R) space is given in [11].

As the Reynolds number is increased from zero to infinity the on-axis critical point moves from $\xi_c \to 0$ to $\xi_c \to \infty$. At these limits the invariants of the on-axis critical point are as indicated in Figure 1. See Section 5 for the coordinates of a, b, c and d. At a first bifurcation Reynolds number of 5.5, $(R_M, Q_M) = (0, 0)$, the on-axis critical point changes from a stable node [5, figure 1c and 7, figure 4a] to a saddle and an off-axis stable node [5, figure 2c and 7, figure 4b]. At a second bifurcation Reynolds number of 7.545, $(R_M, Q_M) = (0, 9/16)$, the off-axis node becomes a stable focus [5, figure 3c and 7, figure 5]. The axisymmetry of the

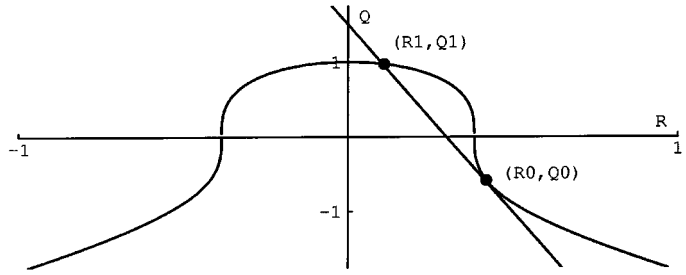

Figure 2. Construction used to find rational roots on a contour of constant D.

flow can be used to show that the on-axis critical point must remain on the curve $D_A = 0$; $D_M = 0$ while the off-axis critical point follows the straight line

$$R_A + \frac{1}{2}Q_A + \frac{1}{8} = 0; \quad R_M = 0. \tag{17}$$

Note that the vector field of particle paths near the off-axis critical point is intrinsically two-dimensional whereas the velocity vector field is not.

4. Elliptic Curves

It is interesting to note the prevalence of rational fractions at the various intersections of the invariant trajectories shown in Figure 1. Note also the mixture of quadratic and cubic terms in the expressions for the discriminant, (15) and (16). For constant discriminant, these equations belong to a class of functions called elliptic curves. The complete classification of cubics, of which elliptic curves is a subset, was described by Isaac Newton in 1695. Elliptic curves have the property that there is a unique tangent everywhere on the curve, hence $D = 0$ is excluded, and they are parameterized by elliptic functions (see, for example, [15]). The curve $D = 0$, which has a cusp at the origin, is parameterized by a rational function as shown in [15]. The most familiar example of an elliptic function comes up in the integral for the arc length of an ellipse although the ellipse itself is not an elliptic curve, it too being parameterized by rational functions.

Elliptic curves come up, for example, in the study of the motions which can be executed by mechanical linkages. Some examples can be found in the classic text by Hunt [12]. They are also of intrinsic mathematical interest and an introductory discussion can be found in the article by Ribet and Hayes [13]. One of the interesting properties of these functions is that a straight line tangent to a rational root intersects the function at another rational root (this works for $D = 0$ too, cf. the intersections of (14), (15) and (16) in Figures 1a and 1b).

This fact can be exploited to create a geometrical construction (Figure 2) by which all rational roots lying on a curve of constant discriminant can be determined once a single root is known.The discriminant has the same value at both points of intersection in Figure 2,

$$Q_1^3 + \frac{27}{4}R_1^2 = Q_0^3 + \frac{27}{4}R_0^2 \tag{18}$$

and the straight line is

$$R + aQ + b = 0. \tag{19}$$

At (R_0, Q_0) the straight line and line of constant D have the same slope as well as the same coordinates. This is used to evaluate a and b and the equation of the straight line is

$$R + \left(\frac{2}{9}\frac{Q_0^2}{R_0}\right) Q + \left(-\frac{2}{9}\frac{Q_0^3}{R_0} - R_0\right) = 0. \tag{20}$$

Now evaluate (20) at (R_1, Q_1) and use it to replace R_1 in (18). The result is a cubic equation for Q_1 which can be factored as

$$(Q_1 - Q_0)^2 \left(Q_1 + \frac{1}{3}\frac{Q_0^4}{R_0^2} + 2Q_0\right) = 0. \tag{21}$$

Two of the roots coincide with the tangent point. The third root combined with (20) leads to

$$\left.\begin{aligned} Q_1 &= -\frac{1}{3}\frac{Q_0^4}{R_0^2} - 2Q_0 \\ R_1 &= \frac{2}{27}\frac{Q_0^6}{R_0^3} + \frac{2}{3}\frac{Q_0^3}{R_0} + R_0 \end{aligned}\right\}. \tag{22}$$

It is clear that if Q_0 and R_0 are rational numbers then so are Q_1 and R_1. Repeating the chord-tangent construction at the new root leads to a third rational root and so on.

5. Topology of the Acceleration Vector Field

Let us use this approach to explore the nature of flow forces at the critical points of the jet. Take the gradient of the incompressible Navier–Stokes equations

$$\frac{\partial}{\partial x_j}\left(\frac{\partial u_i}{\partial t} + u_k\frac{\partial u_i}{\partial x_k}\right) = \frac{\partial}{\partial x_j}\left(-\frac{1}{\rho}\frac{\partial p}{\partial x_i} + \nu\frac{\partial^2 u_i}{\partial x_k \partial x_k}\right). \tag{23}$$

The trace of (23) gives the Poisson equation for the pressure. This is then subtracted from (23) to produce the transport equation for the velocity gradient tensor

$$\frac{Da_j^i}{Dt} + a_k^i a_j^k - \frac{1}{3}\left(a_n^m a_m^n\right)\delta_j^i = h_j^i, \tag{24}$$

where

$$h_j^i = -\left(\frac{1}{\rho}\frac{\partial^2 p}{\partial x_i x_j} - \frac{1}{\rho}\frac{\partial^2 p}{\partial x_k \partial x_k}\frac{\delta_j^i}{3}\right) + \nu\frac{\partial^2 a_j^i}{\partial x_k \partial x_k}. \tag{25}$$

The tensor h_j^i is the divergence free, $(P_h = 0)$, part of the gradient of the acceleration vector field. When (24) is transformed to similarity variables for the round jet the result is

$$-A_j^i + \left(U_k - \frac{1}{2}\xi^k\right)\frac{\partial A_j^i}{\partial \xi^k} + A_k^i A_j^k - \frac{1}{3}\left(A_n^m A_m^n\right)\delta_j^i = H_j^i, \tag{26}$$

where H is given by (25) but is expressed in terms of (A_j^i, P, ξ^i). At a critical point

$$-A_j^i + A_k^i A_j^k - \frac{1}{3}\left(A_n^m A_m^n\right)\delta_j^i = H_j^i. \tag{27}$$

Squaring (27) and taking the trace produces

$$Q_H = -\frac{1}{3}Q_A^2 + Q_A - 3R_A. \tag{28}$$

Cubing (27) and taking the trace produces

$$R_H = -R_A^2 - R_A + Q_A R_A - \frac{2}{3}Q_A^2 - \frac{2}{27}Q_A^3. \tag{29}$$

Now switch over and square (29) and cube (28) to form the discriminant of the acceleration gradient tensor H

$$Q_H^3 + \frac{27}{4}R_H^2 = \left(Q_A^3 + \frac{27}{4}R_A^2\right)(1 + Q_A - R_A)^2. \tag{30}$$

A remarkably simple result! A generalization of this procedure is described in [14]. We can also express the invariants of H in terms of the invariants of M. The result is

$$\left.\begin{aligned} Q_H &= 3Q_M - 3R_M - \frac{1}{3}Q_M^2 - \frac{27}{16} \\ R_H &= -R_M^2 - \frac{9}{4}R_M + 2Q_M R_M - \frac{2}{27}Q_M^3 - \frac{5}{4}Q_M^2 + \frac{9}{4}Q_M - \frac{27}{32} \\ Q_H^3 + \frac{27}{4}R_H^2 &= \left(Q_M^3 + \frac{27}{4}R_M^2 + \frac{27}{4}R_M\left(\frac{1}{2} - Q_M\right) - \frac{9}{16}Q_M^2\right)\left(R_M - \frac{3}{2}Q_M\right)^2 \end{aligned}\right\}. \tag{31}$$

At the off-axis critical point where $R_M = 0$,

$$\left.\begin{aligned} Q_H &= 3Q_M - \frac{1}{3}Q_M^2 - \frac{27}{16} \\ R_H &= -\frac{2}{27}Q_M^3 - \frac{5}{4}Q_M^2 + \frac{9}{4}Q_M - \frac{27}{32} \\ Q_H + \frac{27}{4}R_H^2 &= \frac{9}{4}Q_M^4\left(Q_M - \frac{9}{16}\right) \end{aligned}\right\}. \tag{32}$$

The trajectory of the critical points in the (R_H, Q_H) plane, with that of the off-axis point parameterized by Q_M as in (32), is depicted in Figure 3. Four significant points are labelled in these plots.

Point *a*

This corresponds to the zero Reynolds number (Stokes flow) limit of the jet where there is a single stable node on the jet axis. The invariants of this critical points are:

$$\left.\begin{aligned} (R_A, Q_A) &= \left(\frac{1}{32}, -\frac{3}{16}\right) \\ (R_M, Q_M) &= \left(\frac{1}{16}, \frac{9}{16}\right) \\ (R_H, Q_H) &= \left(-\frac{125}{2048}, -\frac{75}{256}\right) \end{aligned}\right\}. \tag{33}$$

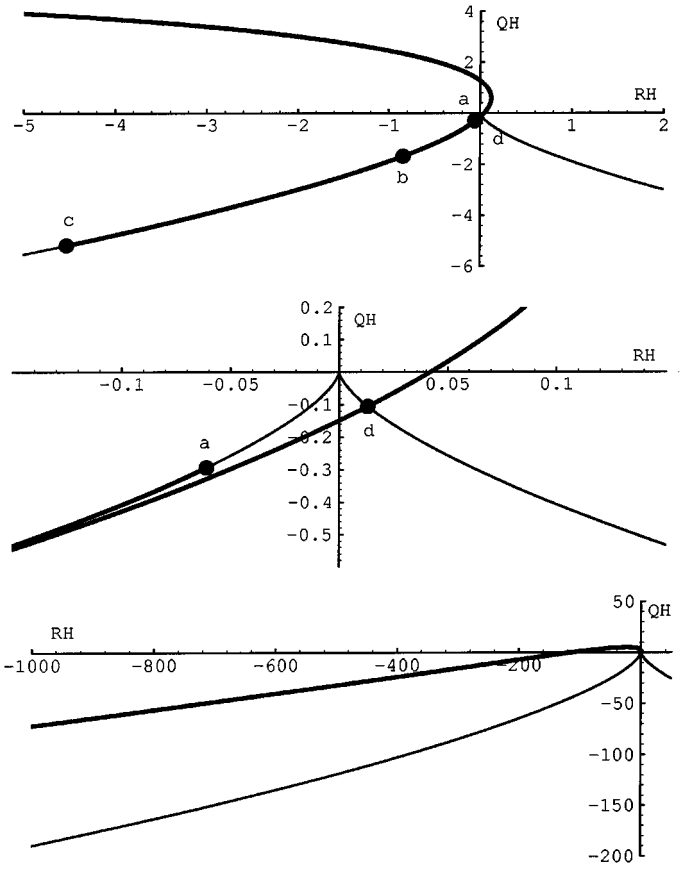

Figure 3. Trajectory of the critical points of the round jet in the (Q_H, R_H) plane at three levels of magnification. Dots indicate several rational roots on the $D_H = 0$ boundary (on-axis critical point) and on the trajectory of the off-axis critical point.

Point *b*

Let the Reynolds number increase. At a critical Reynolds number of 5.5 the jet undergoes a bifurcation to a saddle on the jet axis and a stable node off the axis. The invariants at the bifurcation point are:

$$\left.\begin{aligned} (R_A, Q_A) &= \left(\frac{1}{4}, -\frac{3}{4}\right) \\ (R_M, Q_M) &= (0, 0) \\ (R_H, Q_H) &= \left(-\frac{27}{32}, -\frac{27}{16}\right) \end{aligned}\right\}. \tag{34}$$

Point c

As the jet Reynolds number increases to infinity the on-axis critical point moves to $\xi \to \infty$ and the invariants asymptote to the values given at c.

$$\left.\begin{aligned}(R_A, Q_A) &= \left(\frac{27}{32}, -\frac{27}{16}\right)\\ (R_M, Q_M) &= \left(\frac{1}{8}, -\frac{15}{16}\right)\\ (R_H, Q_H) &= \left(-\frac{9261}{2048}, -\frac{1323}{256}\right)\end{aligned}\right\}. \tag{35}$$

Point d

Above the first bifurcation Reynolds number, the invariants of the off-axis critical point move upward along a straight line $R_M = 0$ until, at a second critical Reynolds number 7.545, the off-axis critical point turns into a saddle node. Thus a starting vortex from the jet is born! The invariants of the off-axis point at this Reynolds number are:

$$\left.\begin{aligned}(R_A, Q_A) &= \left(-\frac{1}{32}, -\frac{3}{16}\right)\\ (R_M, Q_M) &= \left(0, \frac{9}{16}\right)\\ (R_H, Q_H) &= \left(\frac{27}{2048}, -\frac{27}{256}\right)\end{aligned}\right\}. \tag{36}$$

6. Concluding Remarks

This preliminary paper is the first to explicitly demonstrate a direct connection between elliptic curves and three-dimensional fluid flow patterns thus opening up a new area of investigation in both fields.

We learn quite a bit from the analysis. Virtually every interesting intersection (bifurcation) in this problem coincides with a rational root in the plane of invariants. Note that the rational roots on the trajectory of the off-axis critical point in (Q_H, R_H) generated by (32) and depicted in Figure 3 are densely spaced just as they are on the real line. Moreover they coincide with rational values of the discriminant. This can be exploited to identify at least one rational root on any curve of constant discriminant derived from a rational value of Q_M and intersected by (32).

The terms of 6th order in Q_A or Q_M which would be expected when the discriminant of H is formed in (30) and (31) have cancelled producing a quintic polynomial in Q for the discriminant in (30) and (31). This has interesting implications for the limiting behavior of the off-axis critical point which, in relative terms, becomes more and more isotropic as $R_e \to \infty$. The signs of the discriminant of all three tensors are the same. Thus if M has complex eigenvalues, so have H and A. Finally, the invariants of the on-axis critical point have finite, rational values as the limit $R_e \to \infty$ is taken. Few such infinite Reynolds number

limits are known in fluid mechanics. A detailed example of the relationship between elliptic curves, elliptic functions and fluid mechanics can be found in [15].

Acknowledgement

Finally, I would like to dedicate this paper to Nail Ibragimov on the occasion of his 60th birthday and in recognition of his outstanding contributions to Modern Group Analysis which have inspired generations of students and researchers throughout the world.

References

1. Blackburn, H. M., Mansour, N. N., and Cantwell, B. J., 'Topology of fine-scale motions in turbulent channel flow', *Journal of Fluid Mechanics* **310**, 1996, 269–292.
2. Soria, J., Sondergaard, R., Cantwell, B., Chong, M., and Perry, A., 'A study of the fine-scale motions of incompressible time-developing mixing layers', *Physics of Fluids* **6**, 1994, 871–884.
3. Chacin, J. M. and Cantwell, B. J., 'Study of turbulence structure using the invariants of the velocity gradient tensor', Department of Mechanical Engineering, Stanford University Report No. TF-70, 1997.
4. Chong, M. S., Soria, J., Perry, A. E., Chacin, J., Cantwell, B. J., and Na, Y., 'Turbulence structures of wall-bounded shear flows using DNS data', *Journal of Fluid Mechanics* **357**, 1998, 225–247.
5. Cantwell, B. J., 'Discriminant based analysis of the dynamics of unsteady flow', in *Joint ISAMM/FRD Interdisciplinary workshop on Symmetry Analysis and Mathematical Modeling*, N. H. Ibragimov and E. A. Lottering (eds.), Foundation for Research Development, Pretoria, South Africa, 1998, pp. 136–150.
6. Cantwell, B. J., 'Transition in the axisymmetric jet', *Journal of Fluid Mechanics* **104**, 1981, 369–386.
7. Cantwell, B. J. and Allen, G. A., 'Transition and mixing in impulsively started jets and vortex rings', in *Proceedings IUTAM Symposium on Turbulence and Chaotic Phenomena in Fluids*, Kyoto, Japan, T. Tatsumi (ed.), Elsevier, Amsterdam, 1984, pp. 123–132.
8. Allen, G. A. and Cantwell, B. J., 'Transition and mixing in impulsively started jets and vortex rings', NASA CR 3893, 1986.
9. Cantwell, B. J., 'Viscous starting jets', *Journal of Fluid Mechanics* **173**, 1986, 159–189.
10. Cantwell, B. J., 'Organized motion in turbulent flow', *Annual Review on Fluid Mechanics* **13**, 1981, 457.
11. Chong, M. S., Perry, A. E., and Cantwell, B. J., 'A general classification of three-dimensional flow fields', *Physics of Fluids A* **2**, 1990, 765–777.
12. Hunt, K. H., *Kinematic Geometry of Mechanisms*, Oxford Engineering Science Series 7, Clarendon Press, Oxford.
13. Ribet, K. A. and Hayes, B., 'Fermat's last theorem and modern arithmetic', *American Scientist* **82**, 1994, 144–156.
14. Cantwell, B. J., 'On the behavior of velocity gradient tensor invariants in direct numerical simulations of turbulence', *Physics of Fluids A* **5**(8), 1993, 2008–2013.
15. Cantwell, B. J., 'Exact solution of a restricted Euler equation for the velocity gradient tensor', *Physics of Fluids A* **4**, 1992, 782–793.